Letter

Truncation-dependent $\mathcal{PT}$ phase transition for the edge states of a two-dimensional non-Hermitian system

Dali Cheng,[1,2] Bo Peng,[2] Meng Xiao,[3] Xianfeng Chen,[2,4,5,6] Luqi Yuan,[2,*] and Shanhui Fan[1]

[1]*Ginzton Laboratory and Department of Electrical Engineering, Stanford University, Stanford, California 94305, USA*

[2]*State Key Laboratory of Advanced Optical Communication Systems and Networks, School of Physics and Astronomy, Shanghai Jiao Tong University, Shanghai 200240, China*

[3]*School of Physics and Technology, Center for Nanoscience and Nanotechnology, and Key Laboratory of Artificial Micro- and Nano-Structures of Ministry of Education, Wuhan University, Wuhan 430072, China*

[4]*Shanghai Research Center for Quantum Sciences, Shanghai 201315, China*

[5]*Jinan Institute of Quantum Technology, Jinan 250101, China*

[6]*Collaborative Innovation Center of Light Manipulation and Applications, Shandong Normal University, Jinan 250358, China*

(Received 16 January 2022; revised 19 April 2022; accepted 25 April 2022; published 6 May 2022)

We consider a bulk system supporting parity and time reversal (PT) symmetry, and investigate how the PT phase transition of edge states is influenced by different truncations of the system. As an example, we study a two-dimensional PT-symmetric Su–Schrieffer–Heeger lattice with non-Hermitian onsite potentials. We find that when the truncation preserves certain symmetries of the bulk lattice, the edge states can remain in the PT-unbroken phase when the non-Hermitian onsite potentials are less than a nonzero critical value. On the other hand, when the truncation removes such symmetries, edge states with complex eigen-energies are observed for infinitesimal non-Hermitian onsite potentials. We develop an analytic theory to account for such behaviors. Our results are important in the manipulation of the gain and loss behaviors of edge states in non-Hermitian systems, with potential applications in the study of topological lasers, quantum sensors, and unidirectional invisibility.

DOI: 10.1103/PhysRevB.105.L201105

A finite-sized physical system may support edge states localized at the boundaries of its bulk. These states play an important role in determining the physical properties of finite-sized physical systems [1–3]. In the field of photonics, edge states can be found in a wide variety of systems, including photonic crystals, metamaterials, and plasmonic structures [4–7]. These states find applications for the guiding of light in information and sensing applications [8,9].

Recently, physical systems with parity and time reversal (PT) symmetries have generated significant interest [10–14]. In particular, bulk periodic systems with PT symmetries have been extensively studied [15–23], and it was noted that these systems can feature a PT phase transition between a PT-unbroken phase with a real eigen-spectrum, and a PT-broken phase with a complex eigen-spectrum [15,16,18–20,23,24]. Since these systems, when truncated, may support edge states, it should be of interest to explore the possible PT phase transitions for the edge states, and to contrast the phase-transition behaviors between the bulk and the edge states. Thus, there have been many results on edge (and interface) states in one-dimensional PT-symmetric systems [25–43]. Edge states in two-dimensional (2D) PT-symmetric systems have also been explored, and both PT-broken and PT-unbroken phases have been observed in different systems [44–49]. In two dimensions, different truncations of the same periodic system can lead to different boundary geometries. However, there has not been an investigation of how the PT phase transition behaviors of edge states in 2D systems are influenced by different truncations.

In this Letter, we show that different PT phase-transition behaviors of edge states can be achieved by varying the truncation of a 2D periodic system. As an illustration, we study a 2D PT-symmetric Su–Schrieffer–Heeger (SSH) lattice with non-Hermitian onsite potentials, and we truncate the lattice in different orientations. These truncations usually lead to localized edge states. We find that when the truncation features certain symmetries, the associated edge states can be in the PT-unbroken phase when the strength of the non-Hermitian onsite potential is small. On the other hand, for a truncation without such symmetries, the edge states always have complex eigen-energies for any infinitesimal strength of the non-Hermitian onsite potential. Our result provides an understanding of the interplay between boundary geometries and eigenstate properties in non-Hermitian systems, and may be useful in the design and engineering of edge states in various photonic applications such as the design of topological lasers [50–52].

We start our theoretical analysis by considering a non-Hermitian 2D SSH lattice, as shown in Fig. 1(a). The lattice is periodic along both x and y directions, and a primitive cell contains four inequivalent lattice sites, which are indicated with coordinates (xa, ya), $[(x+1/2)a, ya]$, $[xa, (y+1/2)a]$, and $[(x+1/2)a, (y+1/2)a]$, respectively ($x, y \in \mathbb{Z}$, and a is the lattice constant). The intracell and intercell coupling strengths are denoted by g_1 and g_2, respectively. Both g_1 and g_2 are assumed to be real. Gain and loss with the same magnitude

*yuanluqi@sjtu.edu.cn

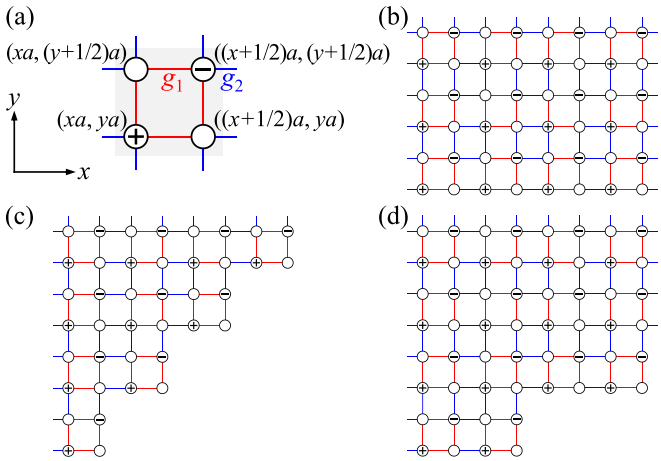

FIG. 1. Two-dimensional SSH lattices and different truncation configurations. (a) A primitive cell of the 2D SSH lattice, as shaded in gray. Intracell (intercell) couplings are shown in red (blue), and gains (losses) are shown by plus (minus) signs. (b)–(d) 2D SSH lattices with the (b) (10), (c) (11), and (d) (21) truncation configurations.

$U \geqslant 0$ in their strength are introduced on $(xa,\ ya)$ sites and on $[(x+1/2)a,\ (y+1/2)a]$ sites, respectively. The Hamiltonian of such system is $H = H_0 + V$, where

$$\begin{aligned} H_0 = & \sum_{x,y} [g_1 (b^\dagger_{x+1/2,y} + b^\dagger_{x,y+1/2})(b_{x,y} + b_{x+1/2,y+1/2}) \\ & + g_2 (b^\dagger_{x+1/2,y+1} + b^\dagger_{x+1,y+1/2})(b_{x+1,y+1} + b_{x+1/2,y+1/2}) \\ & + \text{h.c.}], \\ V = & iU \sum_{x,y} (b^\dagger_{x,y} b_{x,y} - b^\dagger_{x+1/2,y+1/2} b_{x+1/2,y+1/2}), \end{aligned} \tag{1}$$

where $b\,(b^\dagger)$ is the bosonic annihilation (creation) operator at the corresponding lattice site. Here $H_0\,(V)$ gives the Hermitian (anti-Hermitian) part of the Hamiltonian—i.e., $H_0 = H_0{}^\dagger$ and $V = -V^\dagger$. The full Hamiltonian is PT symmetric—i.e., $(PT)^{-1} H (PT) = H$—where the parity operator P is defined as the inversion operation around the point $[(x+1/4)a,\ (y+1/4)a]$, and T is the standard time-reversal operation. The corresponding band structure of this Hamiltonian is

$$\begin{aligned} E(k_x, k_y) = & \pm \sqrt{|g_1 + g_2 \exp(ik_x a)|^2 - \frac{U^2}{4}} \\ & \pm \sqrt{|g_1 + g_2 \exp(ik_y a)|^2 - \frac{U^2}{4}}, \end{aligned} \tag{2}$$

where $k_x\,(k_y)$ is the wave vector along the x (y) axis. The band structure for $U = 0$, $g_1 = g$, and $g_2 = 5g$ is plotted in Fig. 2(a). Four bands are observed because each primitive cell contains four sites. The two middle bands are degenerate at zero energy when $k_x = \pm k_y$, and they are gapped from the other two bands. As seen in Eq. (2), there is a phase transition occurring at a critical value of $U_C^{\text{bulk}} = 2|g_1 - g_2|$. When $U \leqslant 2|g_1 - g_2|$, the energy spectrum is real throughout the entire reciprocal space. When $U > 2|g_1 - g_2|$, the energy spectrum becomes complex for at least some of the wave vectors, and the system undergoes a phase transition entering the PT-broken phase.

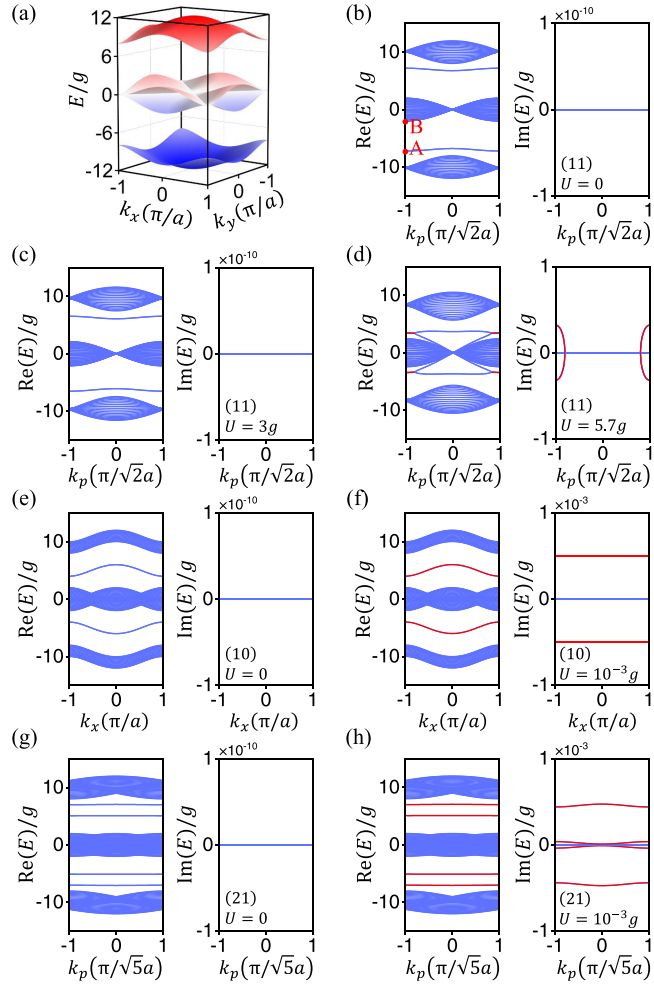

FIG. 2. Band structures of periodic and truncated 2D SSH lattices when $g_1 = g$, $g_2 = 5g$. (a) Band structure of periodic (bulk) 2D SSH lattice. (b)–(d) Projected band structures of a 2D SSH lattice with a (11) truncation when (b) $U = 0$, (c) $U = 3g$, and (d) $U = 5.7g$. (e) and (f) Projected band structures of a 2D SSH lattice with a (10) truncation when (e) $U = 0$ and (f) $U = 10^{-3}g$. (g) and (h) Projected band structures of a 2D SSH lattice with a (21) truncation when (g) $U = 0$ and (h) $U = 10^{-3}g$. In (b)–(h), $N = 21$ layers of primitive cells along the y direction are used for numerical calculations, instead of the semi-infinite lattices in Fig. 1(b)–1(d). Eigen-energies with nonzero imaginary parts are in red.

A one-dimensional SSH lattice is well known as one of the simplest topological models [53]. With certain choices of parameters, the periodic lattice exhibits a nonzero Zak phase [54], which guarantees localized edge states when the lattice is truncated. For the 2D case considered here, there is also a nonzero Zak phase along any direction inside the Brillouin zone when $g_2 > g_1$. Here, the vectorized Zak phase for the 2D Hermitian SSH model is defined as [55,56]

$$\theta = -\frac{1}{2\pi} \int_{\text{BZ}} d^2\mathbf{k} \sum_n i \langle u_n(\mathbf{k}) | \nabla_{\mathbf{k}} | u_n(\mathbf{k}) \rangle, \tag{3}$$

where $|u_n(\mathbf{k})\rangle$ is the periodic part of the Bloch wavefunction of the nth band in the reciprocal space [55]. The summation

is taken over all bands. The jth component of the vectorized Zak phase is

$$\theta_j = 2\int_{-\pi/a}^{\pi/a} dk_j \frac{\partial}{\partial k_j} \arg(g_1 + g_2 e^{ik_j a}), \quad j = x, y. \tag{4}$$

The quantity $f(k_j) = g_1 + g_2 e^{ik_j a}$ lies in a complex plane. For $g_2 < g_1$, the origin of the complex plane is outside the circle defined by $f(k_j)$ as k_j varies across the Brillouin Zone from $-\pi/a$ to π/a, and θ_j is zero, while for $g_2 > g_1$, the origin is inside the circle, giving rise to a nonzero θ_j. Thus, there are also localized edge states with a topological origin. In particular, for the lattice that we consider, when the Zak phase is nonzero, all the edge states inside the gap in our model have a topological origin. Moreover, there is an additional richness in the edge state behaviors since we can choose different orientations for the truncation of the lattice. In Fig. 1(b)–1(d), we provide an illustration of three truncation configurations as examples. The truncations are set to be (10) surface [Fig. 1(b), parallel to the $\hat{\mathbf{x}}$ direction], (11) surface [Fig. 1(c), parallel to the $\hat{\mathbf{x}} + \hat{\mathbf{y}}$ direction], and (21) surface [Fig. 1(d), parallel to the $2\hat{\mathbf{x}} + \hat{\mathbf{y}}$ direction]. In all of the three truncations, the four-site primitive cell structure is preserved on the boundaries of lattices.

Throughout the Letter, we present a theoretical analysis for semi-infinite structures with a single truncation. In the numerical analysis, however, we present results on large finite stripes, which are shown in Fig. 2. The Hamiltonian that we analyze in this Letter does not have a nontrivial point gap topology, and hence does not exhibit non-Hermitian skin effects [57–60]. Therefore, the results from a large finite stripe are rather similar to those from the corresponding semi-infinite system. In the finite stripe, we have pairs of edge states residing on either end of the stripe, and the spectrum of each member of the pair is essentially identical to that of the edge state in the semi-infinite system.

The truncated SSH lattices in Fig. 1(b)–1(d) has translational symmetry only in one direction, and the associated projected band structures are shown in Fig. 2(b)–2(h) in the topologically nontrivial phase ($g_1 = g,\ g_2 = 5g$). Projected band structures of Hermitian systems ($U = 0$) are plotted in Fig. 2(b), 2(e), and 2(g) with different truncation configurations. There, k_p is the wave vector parallel to the truncation. In these projected band structures, the bulk states can be obtained by projecting the 2D band structure as shown in Fig. 2(a) onto appropriate lines in the reciprocal space and by performing band folding if necessary. In such projections, $k_p = k_x$ for the (10) truncation, $k_p = (k_x + k_y)/\sqrt{2}$ for the (11) truncation, and $k_p = (2k_x + k_y)/\sqrt{5}$ for the (21) truncation. These bulk states are separated by band gaps. Moreover, isolated edge states are observed inside the band gaps. Both the (10) and (11) truncations have two edge states, while the (21) truncation features four; thus, the number of edge states is dependent on the lattice truncation [61].

Next, we move on to the non-Hermitian case ($U > 0$). Earlier we showed that the bulk band structure undergoes a PT phase transition at $U_C^{\text{bulk}} = 2|g_1 - g_2|$. Here we show that the edge states also undergo a phase transition, but the transition behaviors are distinctly different from the bulk and are dependent critically on the orientations of the truncations. Figure 2(f) and 2(h) gives the projected band structures of non-Hermitian lattices for the (10) and (21) truncations, respectively, with $U = 10^{-3}g$. One sees that the energies of edge states exhibit nonzero imaginary parts across the entire k-space. The eigen-energies of the bulk states, on the other hand, remain real valued. In other words, for the edge states associated with the (10) and (21) truncations, the phase transition occurs at an infinitesimal strength of non-Hermiticity, and the critical values are $U_C^{(10)} = U_C^{(21)} = 0$. This result of the (10) truncation is consistent with previous literature [48].

The projected band structures of the (11) truncation are shown in Fig. 2(c) and 2(d) with different values of the non-Hermiticity strength U. In contrast to the (10) and (21) truncations, here the eigen-energies of all edge states are still real when $U = 3g$. As the non-Hermiticity strength is further increased and reaches $U_C^{(11)} \approx 5.65g$, the edge states merge with the highest energy bulk states in the middle bands near $|k_p| = \pm\pi/\sqrt{2}a$, and a phase transition occurs. In Fig. 2(d), the projected band structure when $U = 5.7g$ is plotted, the eigen-energies of the edge states become complex in the wave vector range of $|k_p| < 0.81\pi/\sqrt{2}a$, and exceptional points are found at $|k_p| \approx 0.81\pi/\sqrt{2}a$. This phase transition with a nonzero critical value is unique to the (11) truncation; for this system, any other (mn) boundary truncation ($m \neq n,\ m, n \in \mathbb{Z}$) has $U_C = 0$.

In order to understand the different behaviors of the edge states for different truncations, next we provide theoretical arguments from the perspective of symmetry analysis. The semi-infinite non-Hermitian systems with (10) and (21) truncations are not PT symmetric for any spatial symmetry operation P. Thus, generically, the energy eigenvalues become complex with infinitesimal non-Hermiticity strength. On the other hand, for the system with the (11) truncation, although the PT symmetry associated with the inversion operation in the 2D bulk SSH lattice disappears, the system has a reflection and time reversal (RT) symmetry, where R is the mirror symmetry associated with the reflection operation against the $\hat{\mathbf{x}} - \hat{\mathbf{y}}$ direction.

The behavior of the edge states for the (11) truncation is directly related to the symmetry property of the lattice. In the lattice with the (11) truncation, when $U = 0$, we use $|\phi_0\rangle$ and $|\phi_1\rangle$ to denote the edge and corresponding bulk states, respectively, involved in the phase transition at a specific k_p point. Here, both $|\phi_0\rangle$ and $|\phi_1\rangle$ are eigenstates of the Hermitian part of the Hamiltonian, as denoted by $H_0^{(11)}$, and the chosen bulk state $|\phi_1\rangle$ is the state exactly at the edge of the gap. In Fig. 3, we plot the distributions of $|\phi_i\rangle$ at $k_p = \pm\pi/\sqrt{2}a$, where the edge state $|\phi_0\rangle$ has odd RT symmetry and the bulk state $|\phi_1\rangle$ has even RT symmetry. Next, to simplify the notation, we suppress the superscripts (11) with the understanding that the Hamiltonian refers to that of a truncated lattice rather than the bulk Hamiltonian in Eq. (1).

As a simple model, we describe the phase transition process in the Hilbert space spanned by $|\phi_0\rangle$ and $|\phi_1\rangle$, with the matrix elements of the Hamiltonian in this Hilbert space calculated as

$$H_{ij} = \langle\phi_i|H_0 + V|\phi_j\rangle = E_j\delta_{ij} + \langle\phi_i|V|\phi_j\rangle, \quad i, j = 0,\ 1. \tag{5}$$

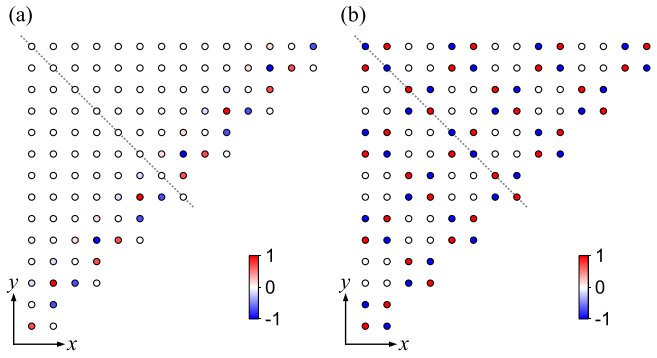

FIG. 3. Eigenstate distributions with the (11) truncation with RT symmetry. (a) The edge state at point A in Fig. 2(b). The state is antisymmetric against the gray dashed line. (b) The bulk state at point B in Fig. 2(b). The state is symmetric against the gray dashed line. The eigenstate magnitudes on lattice sites are normalized with respect to the maximum value in the whole lattice.

In Eq. (5), E_i is the eigen-energy for the state $|\phi_i\rangle$. The last term, $V_{ij} = \langle\phi_i|V|\phi_j\rangle$, arises from the gain or loss added to the lattice sites. By noticing that $V^\dagger = -V$, one can obtain

$$\langle\phi_i|V|\phi_j\rangle^* = \langle\phi_j|V^\dagger|\phi_i\rangle = -\langle\phi_j|V|\phi_i\rangle. \tag{6}$$

Therefore, we have $V_{ii}^* = -V_{ii}$, so V_{ii} is purely imaginary. Also, the off-diagonal elements of the coupling matrix can be written as

$$V_{01} = (\gamma + i\kappa)U, \quad V_{10} = (-\gamma + i\kappa)U, \quad \gamma, \kappa \in \mathbb{R}, \tag{7}$$

where γ and κ are independent of the strength of the non-Hermiticity U. Since the lattice with the (11) truncation has RT symmetry, we have

$$(RT)^{-1}H_0(RT) = H_0, \tag{8}$$

$$(RT)^{-1}V(RT) = V. \tag{9}$$

Because of Eq. (8), the nondegenerate eigenstates of H_0 satisfy

$$RT|\phi_i\rangle = r_i|\phi_i\rangle, \quad r_i = \pm 1, \quad i = 0, 1. \tag{10}$$

By combining Eqs. (9) and (10), we have

$$\begin{aligned} r_j\langle\phi_i|V|\phi_j\rangle &= \langle\phi_i|VRT|\phi_j\rangle = \langle\phi_i|RTV|\phi_j\rangle \\ &= \langle RT\phi_i|V|\phi_j\rangle^* = r_i\langle\phi_i|V|\phi_j\rangle^*, \end{aligned} \tag{11}$$

which indicates that V_{ii} is real. V_{ii} is both real and purely imaginary, so one concludes

$$V_{ii} = 0. \tag{12}$$

Also, since for our system $r_0 = -r_1$, we have $V_{10} = -V_{10}^*$. Therefore, combining with Eq. (7), we have

$$V_{01} = V_{10} = i\kappa U. \tag{13}$$

Therefore, from Eqs. (5), (12), and (13), we obtain a matrix form of the Hamiltonian

$$H = \begin{bmatrix} E_0 & i\kappa U \\ i\kappa U & E_1 \end{bmatrix}, \tag{14}$$

and its eigenvalues are

$$E_\pm = \frac{E_0 + E_1}{2} \pm \frac{\sqrt{(E_0 - E_1)^2 - 4\kappa^2 U^2}}{2}. \tag{15}$$

From Eq. (15), one finds that, when $0 < U \leqslant U_C = \min_{k_p} |E_0 - E_1|/(2\kappa)$, both the edge state and the bulk state remain real-valued energies. Moreover, when the dimerization ratio g_2/g_1 becomes larger, $|E_0 - E_1|$ increases, and therefore the critical value of the PT phase transition U_C increases.

Our results point to a connection between a nonzero critical value of phase transition in Eq. (15), and the existence of RT symmetry for both H_0 and V [Eqs. (8) and (9)]. In our system, lattices with truncations other than (11) do not exhibit RT symmetry, and hence the phase transition occurs at infinitesimal strength of the non-Hermiticity. Such an approach based on symmetry analysis could be applied to other non-Hermitian 2D systems as well. For example, we can numerically verify the PT phase transition of the strained graphene lattice with onsite gains and losses as studied in [47]. With the bearded or zigzag truncations, the honeycomb lattice does not feature any RT symmetry, and the lattice is in the PT-broken phase for infinitesimal strength of the non-Hermiticity when edge states are present. The lattice with the armchair truncation has an additional RT symmetry and hence a nonzero critical value U_C for the phase transition. For the armchair truncation for this system, there is no edge state; thus, the phase transition occurs through the coalescence of two bulk states. The edge states considered here have topological origins, but their PT phase-transition behaviors are not directly and causally related to the topological properties, since the topological properties are determined by the bulk Hamiltonian, whereas the properties of the PT phase transition are affected by the symmetries of the truncations. The importance of symmetry consideration in PT phase transition has been noted in a number of studies on some one-dimensional [30] and two-dimensional [46] lattices, or more generally on wave equations [62] and topological many-body systems [63] with degeneracy. Our work differs in that we use the symmetry analysis to study the dependence of the phase transition of the edge states on the lattice truncations.

In summary, we investigate the truncation dependence of the PT phase transition of edge states in a 2D physical system where the bulk periodic system has PT symmetry. Our results show that, with specific truncation configurations [such as the (11) truncation], the truncated system preserves certain symmetry properties of the bulk periodic system, and consequently the critical value of the PT phase transition is nonzero for the edge states. The edge states remain in the PT-unbroken phase when the non-Hermiticity is within the critical value. For other configurations where the truncation breaks the symmetry of the bulk, the eigen-energies exhibit nonzero imaginary parts, and edge states experience gain and loss for infinitesimal non-Hermiticity. Our theoretical study is applicable to a variety of experimental platforms that have been used to construct two-dimensional periodic lattices, such as photonic waveguide arrays, resonator arrays and cavity arrays [64–68], cold bosonic atoms in optical lattices [69,70], superconducting circuits [71–73], and artificial lattices with synthetic dimensions [74–78]. The results and arguments presented in this Letter are expected to provide insights into

research that requires the engineering of the critical values of the *PT* phase transition of edge states in multidimensional physical systems—for example, in the studies of sensing, topological lasing, and unidirectional invisibility near a *PT* phase-transition point [13,14,79,80].

The authors are grateful for helpful discussions with Prof. Zhong Wang and Dr. Kai Wang. The research is supported by the National Natural Science Foundation of China (Grants No. 12122407 and No. 11974245), the National Key R&D Program of China (Grant No. 2017YFA0303701), the Shanghai Municipal Science and Technology Major Project (Grant No. 2019SHZDZX01), and the Natural Science Foundation of Shanghai (Grant No. 19ZR1475700). L.Y. acknowledges support from the Program for Professor of Special Appointment (Eastern Scholar) at Shanghai Institutions of Higher Learning. X.C. acknowledges support from a Shandong Quancheng Scholarship (Grant No. 00242019024). S.F. acknowledges the support of a Vannevar Bush Faculty Fellowship from the U. S. Department of Defense (Grant No. N00014-17-1-3030) and a Simons Investigator in Physics grant from the Simons Foundation (Award No. 827065).

[1] W. Shockley, On the surface states associated with a periodic potential, Phys. Rev. **56**, 317 (1939).
[2] A. H. Castro Neto, F. Guinea, N. M. R. Peres, K. S. Novoselov, and A. K. Geim, The electronic properties of graphene, Rev. Mod. Phys. **81**, 109 (2009).
[3] M. Z. Hasan and C. L. Kane, *Colloquium*: Topological insulators, Rev. Mod. Phys. **82**, 3045 (2010).
[4] R. D. Meade, K. D. Brommer, A. M. Rappe, and J. D. Joannopoulos, Electromagnetic Bloch waves at the surface of a photonic crystal, Phys. Rev. B **44**, 10961 (1991).
[5] W. L. Barnes, A. Dereux, and T. W. Ebbesen, Surface plasmon subwavelength optics, Nature (London) **424**, 824 (2003).
[6] L. Lu, J. D. Joannopoulos, and M. Soljačić, Topological photonics, Nat. Photonics **8**, 821 (2014).
[7] T. Ozawa *et al.*, Topological photonics, Rev. Mod. Phys. **91**, 015006 (2019).
[8] F. Villa, L. E. Regalado, F. Ramos-Mendieta, J. Gaspar-Armenta, and T. Lopez-Ríos, Photonic crystal sensor based on surface waves for thin-film characterization, Opt. Lett. **27**, 646 (2002).
[9] S. Barik, A. Karasahin, C. Flower, T. Cai, H. Miyake, W. DeGottardi, M. Hafezi, and E. Waks, A topological quantum optics interface, Science **359**, 666 (2018).
[10] C. E. Rüter, K. G. Makris, R. El-Ganainy, D. N. Christodoulides, M. Segev, and D. Kip, Observation of parity–time symmetry in optics, Nat. Phys. **6**, 192 (2010).
[11] A. A. Zyablovsky, A. P. Vinogradov, A. A. Pukhov, A. V. Dorofeenko, and A. A. Lisyansky, PT-symmetry in optics, Phys. Usp. **57**, 1063 (2014).
[12] L. Feng, Z. J. Wong, R.- M. Ma, Y. Wang, and X. Zhang, Single-mode laser by parity-time symmetry breaking, Science **346**, 972 (2014).
[13] L. Feng, R. El-Ganainy, and L. Ge, Non-Hermitian photonics based on parity–time symmetry, Nat. Photonics **11**, 752 (2017).
[14] Ş. K. Özdemir, S. Rotter, F. Nori, and L. Yang, Parity–time symmetry and exceptional points in photonics, Nat. Mater. **18**, 783 (2019).
[15] Z. H. Musslimani, K. G. Makris, R. El-Ganainy, and D. N. Christodoulides, Optical Solitons in PT Periodic Potentials, Phys. Rev. Lett. **100**, 030402 (2008).
[16] K. G. Makris, R. El-Ganainy, D. N. Christodoulides, and Z. H. Musslimani, Beam Dynamics in $\mathcal{PT}$ Symmetric Optical Lattices, Phys. Rev. Lett. **100**, 103904 (2008).
[17] S. Longhi, Bloch Oscillations in Complex Crystals with $\mathcal{PT}$ Symmetry, Phys. Rev. Lett. **103**, 123601 (2009).
[18] Z. Lin, H. Ramezani, T. Eichelkraut, T. Kottos, H. Cao, and D. N. Christodoulides, Unidirectional Invisibility Induced by PT-Symmetric Periodic Structures, Phys. Rev. Lett. **106**, 213901 (2011).
[19] A. Regensburger, C. Bersch, M.- A. Miri, G. Onishchukov, D. N. Christodoulides, and U. Peschel, Parity–time synthetic photonic lattices, Nature (London) **488**, 167 (2012).
[20] M. Wimmer, A. Regensburger, M.- A. Miri, C. Bersch, D. N. Christodoulides, and U. Peschel, Observation of optical solitons in PT-symmetric lattices, Nat. Commun. **6**, 7782 (2015).
[21] M. Wimmer, M.- A. Miri, D. Christodoulides, and U. Peschel, Observation of Bloch oscillations in complex PT-symmetric photonic lattices, Sci. Rep. **5**, 17760 (2015).
[22] Y.-L. Xu, W. S. Fegadolli, L. Gan, M.-H. Lu, X.-P. Liu, Z.-Y. Li, A. Scherer, and Y.- F. Chen, Experimental realization of Bloch oscillations in a parity-time synthetic silicon photonic lattice, Nat. Commun. **7**, 11319 (2016).
[23] Z. Zhang, Y. Zhang, J. Sheng, L. Yang, M.-A. Miri, D. N. Christodoulides, B. He, Y. Zhang, and M. Xiao, Observation of Parity-Time Symmetry in Optically Induced Atomic Lattices, Phys. Rev. Lett. **117**, 123601 (2016).
[24] A. Cerjan, A. Raman, and S. Fan, Exceptional Contours and Band Structure Design in Parity-Time Symmetric Photonic Crystals, Phys. Rev. Lett. **116**, 203902 (2016).
[25] B. Zhu, R. Lü, and S. Chen, PT symmetry in the non-Hermitian Su-Schrieffer-Heeger model with complex boundary potentials, Phys. Rev. A **89**, 062102 (2014).
[26] C. Poli, M. Bellec, U. Kuhl, F. Mortessagne, and H. Schomerus, Selective enhancement of topologically induced interface states in a dielectric resonator chain, Nat. Commun. **6**, 6710 (2015).
[27] C. Yuce, Topological phase in a non-Hermitian PT symmetric system, Phys. Lett. A **379**, 1213 (2015).
[28] X. Wang, T. Liu, Y. Xiong, and P. Tong, Spontaneous PT-symmetry breaking in non-Hermitian Kitaev and extended Kitaev models, Phys. Rev. A **92**, 012116 (2015).
[29] H. Zhao, S. Longhi, and L. Feng, Robust light state by quantum phase transition in non-Hermitian optical materials, Sci. Rep. **5**, 17022 (2015).
[30] A. K. Harter, T. E. Lee, and Y. N. Joglekar, PT-breaking threshold in spatially asymmetric Aubry-André and Harper models: Hidden symmetry and topological states, Phys. Rev. A **93**, 062101 (2016).
[31] S. Weimann, M. Kremer, Y. Plotnik, Y. Lumer, S. Nolte, K. G. Makris, M. Segev, M. C. Rechtsman, and A. Szameit,

Topologically protected bound states in photonic parity–time-symmetric crystals, Nat. Mater. **16**, 433 (2017).

[32] M. Klett, H. Cartarius, D. Dast, J. Main, and G. Wunner, Relation between PT-symmetry breaking and topologically nontrivial phases in the Su-Schrieffer-Heeger and Kitaev models, Phys. Rev. A **95**, 053626 (2017).

[33] L. Jin, P. Wang, and Z. Song, Su-Schrieffer-Heeger chain with one pair of PT-symmetric defects, Sci. Rep. **7**, 5903 (2017).

[34] L. Xiao *et al.*, Observation of topological edge states in parity–time-symmetric quantum walks, Nat. Phys. **13**, 1117 (2017).

[35] L. Jin, Topological phases and edge states in a non-Hermitian trimerized optical lattice, Phys. Rev. A **96**, 032103 (2017).

[36] S. Lieu, Topological phases in the non-Hermitian Su-Schrieffer-Heeger model, Phys. Rev. B **97**, 045106 (2018).

[37] C. Yuce, Edge states at the interface of non-Hermitian systems, Phys. Rev. A **97**, 042118 (2018).

[38] C. Yuce, Stable topological edge states in a non-Hermitian four-band model, Phys. Rev. A **98**, 012111 (2018).

[39] Z.- X. Kong, Y.- F. Zhang, H.- X. Hao, and W.- J. Gong, Energy spectra of coupled Su-Schrieffer-Heeger chains with PT-symmetric imaginary boundary potentials, Phys. Scr. **95**, 115801 (2020).

[40] S. Xia, D. Kaltsas, D. Song, I. Komis, J. Xu, A. Szameit, H. Buljan, K. G. Makris, and Z. Chen, Nonlinear tuning of PT symmetry and non-Hermitian topological states, Science **372**, 72 (2021).

[41] A. Stegmaier *et al.*, Topological Defect Engineering and $\mathcal{PT}$ Symmetry in Non-Hermitian Electrical Circuits, Phys. Rev. Lett. **126**, 215302 (2021).

[42] S. Longhi, PT-symmetric optical superlattices, J. Phys. A Math. Theor. **47**, 165302 (2014).

[43] M. Pan, H. Zhao, P. Miao, S. Longhi, and L. Feng, Photonic zero mode in a non-Hermitian photonic lattice, Nat. Commun. **9**, 1308 (2018).

[44] K. Esaki, M. Sato, K. Hasebe, and M. Kohmoto, Edge states and topological phases in non-Hermitian systems, Phys. Rev. B **84**, 205128 (2011).

[45] Z. Oztas and C. Yuce, Spontaneously broken particle-hole symmetry in photonic graphene with gain and loss, Phys. Rev. A **98**, 042104 (2018).

[46] X. Ni, D. Smirnova, A. Poddubny, D. Leykam, Y. Chong, and A. B. Khanikaev, $\mathcal{PT}$ phase transitions of edge states at $\mathcal{PT}$ symmetric interfaces in non-Hermitian topological insulators, Phys. Rev. B **98**, 165129 (2018).

[47] M. Kremer, T. Biesenthal, L. J. Maczewsky, M. Heinrich, R. Thomale, and A. Szameit, Demonstration of a two-dimensional PT-symmetric crystal, Nat. Commun. **10**, 435 (2019).

[48] C. Yuce and H. Ramezani, Topological states in a non-Hermitian two-dimensional Su-Schrieffer-Heeger model, Phys. Rev. A **100**, 032102 (2019).

[49] S. Fan, Y. Xing, L. Qi, H.-F. Wang, and S. Zhang, Defect-position-dependent PT-symmetry breaking in coupled Su–Schrieffer–Heeger chains, Laser Phys. Lett. **16**, 125203 (2019).

[50] M. Parto, S. Wittek, H. Hodaei, G. Harari, M. A. Bandres, J. Ren, M. C. Rechtsman, M. Segev, D. N. Christodoulides, and M. Khajavikhan, Edge-Mode Lasing in 1D Topological Active Arrays, Phys. Rev. Lett. **120**, 113901 (2018).

[51] A. Y. Song, X.- Q. Sun, A. Dutt, M. Minkov, C. Wojcik, H. Wang, I. A. D. Williamson, M. Orenstein, and S. Fan, PT-Symmetric Topological Edge-Gain Effect, Phys. Rev. Lett. **125**, 033603 (2020).

[52] Z. Chen and M. Segev, Highlighting photonics: Looking into the next decade, eLight **1**, 2 (2021).

[53] W. P. Su, J. R. Schrieffer, and A. J. Heeger, Solitons in Polyacetylene, Phys. Rev. Lett. **42**, 1698 (1979).

[54] J. Zak, Berry's Phase for Energy Bands in Solids, Phys. Rev. Lett. **62**, 2747 (1989).

[55] D. Obana, F. Liu, and K. Wakabayashi, Topological edge states in the Su-Schrieffer-Heeger model, Phys. Rev. B **100**, 075437 (2019).

[56] M. Kim and J. Rho, Topological edge and corner states in a two-dimensional photonic Su-Schrieffer-Heeger lattice, Nanophotonics **9**, 3227 (2020).

[57] C. H. Lee and R. Thomale, Anatomy of skin modes and topology in non-Hermitian systems, Phys. Rev. B **99**, 201103 (2019).

[58] F. K. Kunst and V. Dwivedi, Non-Hermitian systems and topology: A transfer-matrix perspective, Phys. Rev. B **99**, 245116 (2019).

[59] K. Kawabata, K. Shiozaki, M. Ueda, and M. Sato, Symmetry and Topology in Non-Hermitian Physics, Phys. Rev. X **9**, 041015 (2019).

[60] E. J. Bergholtz, J. C. Budich, and F. K. Kunst, Exceptional topology of non-Hermitian systems, Rev. Mod. Phys. **93**, 015005 (2021).

[61] P. Delplace, D. Ullmo, and G. Montambaux, Zak phase and the existence of edge states in graphene, Phys. Rev. B **84**, 195452 (2011).

[62] L. Ge and A. D. Stone, Parity-Time Symmetry Breaking Beyond One Dimension: The Role of Degeneracy, Phys. Rev. X **4**, 031011 (2014).

[63] H. Shackleton and M. S. Scheurer, Protection of parity-time symmetry in topological many-body systems: Non-Hermitian toric code and fracton models, Phys. Rev. Research **2**, 033022 (2020).

[64] A. Yariv, Y. Xu, R. K. Lee, and A. Scherer, Coupled-resonator optical waveguide: A proposal and analysis, Opt. Lett. **24**, 711 (1999).

[65] M. J. Hartmann, F. G. S. L. Brandão, and M. B. Plenio, Strongly interacting polaritons in coupled arrays of cavities, Nat. Phys. **2**, 849 (2006).

[66] D. O. Krimer and R. Khomeriki, Realization of discrete quantum billiards in a two-dimensional optical lattice, Phys. Rev. A **84**, 041807 (2011).

[67] G. Corrielli, A. Crespi, G. Della Valle, S. Longhi, and R. Osellame, Fractional Bloch oscillations in photonic lattices, Nat. Commun. **4**, 1555 (2013).

[68] F. Klauck, M. Heinrich, and A. Szameit, Photonic two-particle quantum walks in Su–Schrieffer–Heeger lattices, Photon. Res. **9**, A1 (2021).

[69] D. Jaksch, C. Bruder, J. I. Cirac, C. W. Gardiner, and P. Zoller, Cold Bosonic Atoms in Optical Lattices, Phys. Rev. Lett. **81**, 3108 (1998).

[70] I. Bloch, J. Dalibard, and W. Zwerger, Many-body physics with ultracold gases, Rev. Mod. Phys. **80**, 885 (2008).

[71] G. Engelhardt, M. Benito, G. Platero, and T. Brandes, Topologically Enforced Bifurcations in Superconducting Circuits, Phys. Rev. Lett. **118**, 197702 (2017).

[72] Z. Yan *et al.*, Strongly correlated quantum walks with a 12-qubit superconducting processor, Science **364**, 753 (2019).

[73] M. Gong *et al.*, Quantum walks on a programmable two-dimensional 62-qubit superconducting processor, Science **372**, 948 (2021).

[74] D. Cheng, B. Peng, D.- W. Wang, X. Chen, L. Yuan, and S. Fan, Arbitrary synthetic dimensions via multiboson dynamics on a one-dimensional lattice, Phys. Rev. Research **3**, 033069 (2021).

[75] A. Celi, P. Massignan, J. Ruseckas, N. Goldman, I. B. Spielman, G. Juzeliūnas, and M. Lewenstein, Synthetic Gauge Fields in Synthetic Dimensions, Phys. Rev. Lett. **112**, 043001 (2014).

[76] L. Yuan, Q. Lin, M. Xiao, and S. Fan, Synthetic dimension in photonics, Optica **5**, 1396 (2018).

[77] A. Dutt, Q. Lin, L. Yuan, M. Minkov, M. Xiao, and S. Fan, A single photonic cavity with two independent physical synthetic dimensions, Science **367**, 59 (2020).

[78] D. Yu, B. Peng, X. Chen, X.- J. Liu, and L. Yuan, Topological holographic quench dynamics in a synthetic frequency dimension, Light Sci. Appl. **10**, 209 (2021).

[79] R. El-Ganainy, K. G. Makris, M. Khajavikhan, Z. H. Musslimani, S. Rotter, and D. N. Christodoulides, Non-Hermitian physics and PT symmetry, Nat. Phys. **14**, 11 (2018).

[80] M.- A. Miri and A. Alù, Exceptional points in optics and photonics, Science **363**, eaar7709 (2019).